Applied Physics Letters

Edge-derived magnetisms in very thin non-doped Bi_2Te_3 nanomesh

Cite as: Appl. Phys. Lett. **115**, 093101 (2019); https://doi.org/10.1063/1.5100024
Submitted: 14 April 2019 . Accepted: 10 August 2019 . Published Online: 27 August 2019

T. Kobayashi, H. Mine, T. Tokuda, Y. Hashimoto, S. Katsumoto, and J. Haruyama

AIP Publishing

Applied Physics Letters ARTICLE scitation.org/journal/apl

Edge-derived magnetisms in very thin non-doped Bi_2Te_3 nanomesh

Cite as: Appl. Phys. Lett. **115**, 093101 (2019); doi: 10.1063/1.5100024
Submitted: 14 April 2019 · Accepted: 10 August 2019 ·
Published Online: 27 August 2019

T. Kobayashi,[1] H. Mine,[1] T. Tokuda,[1] Y. Hashimoto,[2] S. Katsumoto,[2] and J. Haruyama[1,2,a)]

AFFILIATIONS

[1]Faculty of Science and Engineering, Aoyama Gakuin University, 5-10-1 Fuchinobe, Sagamihara, Kanagawa 252-5258, Japan
[2]Institute for Solid State Physics, The University of Tokyo, 5-1-5 Kashiwanoha, Kashiwa, Chiba 277-8581, Japan

[a)]J-haru@ee.aoyama.ac.jp

ABSTRACT

Pristine topological insulators (TIs) with no carrier doping principally suffer from a lack of magnetic ordering. We create a nanomesh structure, a honeycomblike array of hexagonal nanopores with extremely high density, on a nondoped two-dimensional (2D) thin TI (Bi_2Te_3). We observe antiferromagnetism (AFM) in completely hydrogen-terminated nanomeshes, while it is eliminated by ferromagnetism (FM) in completely O-terminated nanomeshes. Interplay between the AFM and FM is observed in partially O-terminated nanomeshes. As a possible origin for the observed magnetisms, Kramers doublets, which may exist around nanopore edges, for AFM and those eliminated by FM spin alignment due to O-Te coupling along pore edges are discussed based on the structure and annealing dependence of the magnetisms. The nondoped 2D nanomesh formed on a TI will lead to new avenues of research on topological magnetisms and spintronics.

Topological insulators (TIs), which represent a nontrivial quantum phase, have attracted significant attention. Various three-dimensional (3D) TIs have been found (e.g., Bi_2Te_3 and Bi_2Se_3), and their electronic behavior has been studied.[1–3] In contrast, because a TI has basically no magnetic ordering, its magnetic properties have mainly been studied via doping with transition metal ions (e.g., Cr,[4–8] Mn,[9–11] and Fe). Some works argued that the long-range ferromagnetic order is independent of the increase in the densities of such ions remaining in the TI states,[5] while others reported the suppression of ferromagnetism (FM) with increasing ion density.[9] The mechanisms behind such FM in 3D TIs have also been debated (e.g., *p*-hole carrier mediation in the host-material lattice with the interaction between the host-*p* and dopant-*d* states[4] and a Dirac-fermion-mediated origin for surface ferromagnetism[9]). However, parasitic problems caused by carrier doping (e.g., defects and contamination) have obstructed the advancement of this research. Thus, it is crucial to produce magnetism in TIs without carrier doping.

Unlike studies of magnetism in 3D TIs, such studies are rare for 2D TIs. In 2D TIs, helical edge spin states, in which edge spins with opposite moments form a Kramers doublet and counterpropagate with time-reversal symmetry (i.e., quantum spin Hall phase), appear. Although this effect has predominantly been researched in 2D semiconductor quantum wells,[12–14] atomically thin layers have recently been demonstrated to be 2D TIs (e.g., WTe_2).[15–17] We have also realized 2D TI states both in graphene decorated with Bi_2Te_3 nanoparticles to coverage levels as low as 3% and in few-layer MoS_2 with a 1T′-phase created using laser beam irradiation.[18–20] Nevertheless, the magnetic behavior caused by helical edge states has never been studied. There is great interest in whether the opposite-moment spins of Kramers doublets can cause antiferromagnetism (AFM) when present in large amounts.

However, the edge volume of conventional 2D materials is very small because this volume exists at only the edge of a sample. Moreover, many defects and considerable contamination exist around edges. These factors have made it difficult to detect the magnetism that arises from the edge spins. Thus, we previously created a 2D thin nanomesh structure with few defects and a low level of contamination using our nonlithographic method, which etches 2D thin bulk layers via a nanoporous alumina template (NPAT) mask on non-TI layers. The large-volume dangling bonds at the zigzag atomic structure's nanopore edges (e.g., pore diameter ∼50 nm and pore density $\sim 10^{11}/cm^2$) with few defects and a low level of contamination in the non-TI nanomesh allowed for the facile observation of various edge-derived magnetisms depending on the material [e.g., graphene,[21,22] black phosphorus,[23] hexagonal boron nitride (hBN),[24] and MoS_2[25]] and the foreign atoms terminating the zigzag pore edges (e.g., O and H). Nevertheless, AFM has never been observed. In the present work, a nanomesh structure is created on a nondoped thin 2D TI (Bi_2Te_3),

and AFM is observed by forming spin instability similar to that of the Kagome lattice[26,27] and causing interplay with edge spin-derived FM.[28–30]

Flakes of thin Bi_2Te_3 are formed by mechanical exfoliation of bulk samples via a Scotch tape method [Fig. 1(a)]. Various flakes exist on one SiO_2/Si substrate {e.g., an area measuring a few ~100 μm^2 and a thickness ranging from a monolayer ~10 layers [Fig. 1(b)]}. 2D TI states are confirmed by the observation of the $R_Q/2$ value (where $R_Q = h/e^2 = 25.8\,k\Omega$ is the quantum resistance) as a function of the back gate voltage (V_{bg}) for the quantum spin Hall effect [Fig. 1(c)] and by the observation of bulk gaps (~90 meV) and the disappearance at the edges by scanning tunneling spectroscopy (STS) [Fig. 1(d)], as well as by our previous experiments on 2D TIs.[17,20] Some theoretical works reported the absence of 2D TI states in thin layers of Bi2Te3,[33] while the presence of 2D TI states was observed experimentally.[34,35] Out results are consistent with the experimental studies. The thick flakes (≫10 nm) are mechanically removed. The NPAT mask is placed on the substrate, and the nanopore array is transferred to the Bi_2Te_3 flakes by low-power Ar gas etching. An example atomic force microscopy image of the formed Bi_2Te_3 nanomesh is shown in Fig. 1(e) (a typical diameter is ~50 nm with an interpore distance of ~20 nm).[31] According to our previous method, the nanomeshes are annealed under high vacuum (10^{-6} Torr) at high temperature (500 °C). Because this temperature is close to the growth temperature of the bulk Bi_2Te_3, edge reconstruction occurs, resulting in the most stable edge atomic structure in terms of the chemical and thermal characteristics. In our previous work, the formation of nanomeshes composed of various materials suggests that the most stable structure has zigzag pore edges. Indeed, annealing at the other temperatures (400 °C and 600 °C) resulted in much less magnetization in O-terminated samples

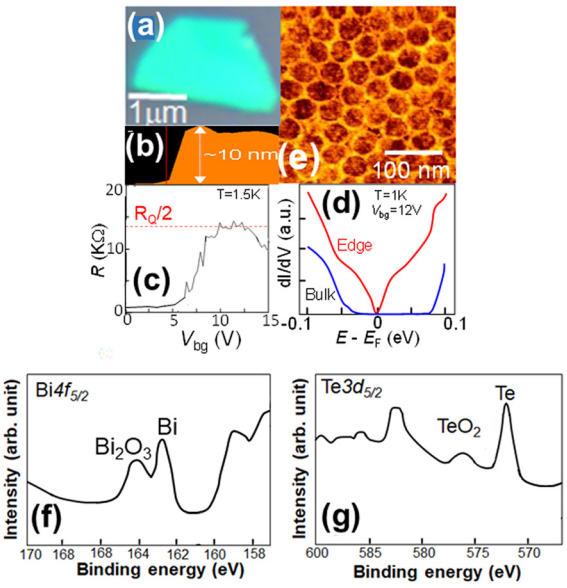

FIG. 1. Sample fabrication and characterization. (a) Optical and (b) cross-sectional atomic force microscopy images of mechanically exfoliated thin Bi_2Te_3 layers. (c) Nonlocal resistance as a function of V_{bg} for four probe measurements of (a). (d) STS measurement of (a). (e) Atomic force microscopy image of thin Bi_2Te_3 nanomeshes. [(f) and (g)] XPS spectra of the oxidized nanomesh sample.

[as shown in Fig. 4(b)], which is analogous to our previous results. Annealing (500 °C) also completely eliminates defects and contamination. Next, the nanomeshes are exposed to air for 2 h or 24 h to establish partially or completely O-terminated pore edges, respectively. To achieve H-termination, the samples are exposed to H radicals. Finally, the NPAT mask is mechanically detached.

Figures 1(d) and 1(e) display X-ray photoelectron spectroscopy (XPS) results for the completely O-terminated nanomesh sample. We confirm the identities of the peaks as Bi (~162 eV) and Bi_2O_3 (~164 eV) in the *Bi4f*$_{5/2}$ orbital and Te (~572 eV) and TeO_2 (~576 eV) in the *Te3d*$_{5/2}$ orbital. The exposure of the nanomesh to air was carried out with the NPAT mask on the surface. Moreover, the interpore distance of the nanomesh is only ~20 nm. Thus, the observed XPS peaks mainly originate from O-termination of the pore edges. These findings indicate the high quality of the pore edges of Bi_2Te_3 nanomeshes, specifically, that the sample possesses few defects and a low level of contamination. In addition, sufficient chemical coupling occurs between the Bi and Te atoms of the pore-edge dangling bonds and the terminating O atoms. The presence of 2D TI states in the nanomeshes cannot yet be confirmed by resistance measurements or STS observations, unlike the case of the bulk material, owing to the extremely small interpore space and the small pore-edge size.

The Bi_2Te_3 nanomeshes on the Si surface (e.g., total area $\lesssim 1 \times 5\,mm^2$) are collected and placed in the tube of a superconducting quantum interference device (Quantum Design; MPMS) for the measurement of the magnetic behavior of the material by the application of an in-plane magnetic field.

The magnetic properties of the Bi_2Te_3 nanomeshes are demonstrated in Fig. 2. Exfoliated pristine thin Bi_2Te_3 flakes (i.e., without nanomeshes) show no magnetization (showing only diamagnetismlike small hysteresis) [Fig. 2(a)]. The temperature (T) dependence of the magnetic susceptibility (χ) of the partially O-terminated nanomesh is shown in Fig. 2(b). This behavior is similar to that of AFM (i.e., χ rapidly increases as T decreases and has a broad peak at approximately $T_{c1} \sim 100$–130 K, whereas at $T < 100$ K, χ gradually decreases toward $\chi = 0$ with decreasing T). Notably, this AFM-like behavior was never observed in our previous nanomeshes formed on various 2D non-TI layers, as mentioned in the introduction. In contrast, χ rapidly increases again at $T < T_{c2} \sim 20$ K with decreasing T. This behavior differs significantly from that of AFM. The typical magnetic curves in individual T regions are shown in Figs. 2(c)–2(f). At $T = 250$ K, a curve indicating paramagnetism (PM) is generated [Fig. 2(c)]. This PM becomes stronger at approximately $T_{c1} = 130$ K [Fig. 2(d)]. In contrast, the χ value of the curve decreases as a small hysteresis loop develops at $T = 50$ K [Fig. 2(e)]. This hysteresis curve becomes more significant as ferromagnetism (FM) becomes apparent at $T = 2$ K [Fig. 2(f)].

Figure 3 demonstrates the T dependence of the χ value of nanomeshes with complete O-termination [Fig. 3(a)] and with complete H-termination [Fig. 3(b)] (i.e., formed by exposing the nanomesh to air or H radicals for 24 h, respectively). AFM (i.e., decreased χ) is absent in Fig. 3(a), and only FM (i.e., monotonically increasing χ) is confirmed. In contrast, FM is absent in Fig. 3(b), and only AFM and PM are confirmed with an evident transition temperature (similar to the Niele temperature) of ~130 K.

Figure 4 shows the correlation of magnetism with (a) the interpore distance (d) and (b) the annealing temperature (T_a) of the completely H- and O-terminated samples. As d decreases, the AFM

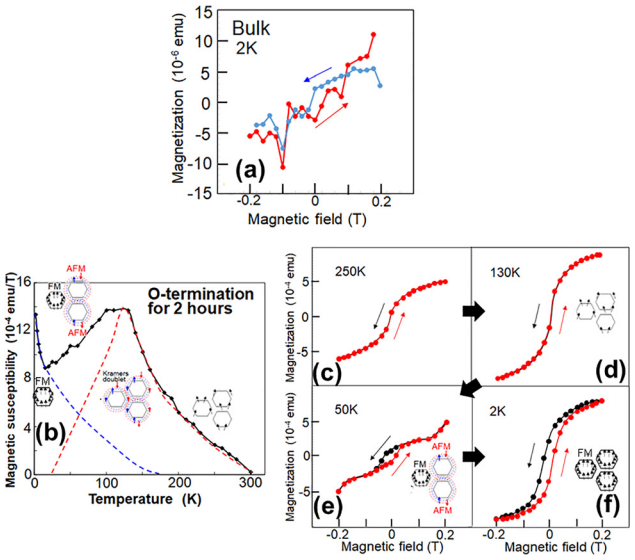

FIG. 2. Magnetization measurements. (a) Magnetization curve of the 2D thin bulk sample without nanopores. (b) Partially O-terminated nanomesh: temperature dependence of the magnetic susceptibility behaviour observed at 100 Oe and (c)–(f) magnetization curves corresponding to the four representative temperature regions in (b). Dashed lines in (b) are used as the guide to the eye and qualitatively correspond to Fig. 3. Magnetic fields are applied in the plane of the nanomesh for all measurements reported in the present manuscript. Insets in (b)–(f): schematic views of the possible pore-edge spin configurations in individual temperature regions [shown by arrows around hexagonal pores; from high temperature, PM, AFM due to Kramers doublets, coexisting FM due to edge O-Te coupling and AFM on different pores, and FM in (b)].

grows unstable in the H-terminated samples (i.e., the magnetization values depart from the minimum values with longer error bars, and the coercivity monotonically decreases), while the magnitude of FM in the O-terminated samples monotonically increases in (a). In (b), the magnitude of FM in the O-terminated samples is maximum at a T_a value of 500 °C, and the AFM in the H-terminated samples becomes most stable (i.e., the magnetization reaches the minimum value with the shortest error bars, and the coercivity reaches the maximum value) after annealing at this T_a. Because of these results, T_a (=500 °C)-annealing was employed for all other samples.

The results shown in Fig. 3 suggest that the results shown in Fig. 2 can be qualitatively attributed to a hybridized state characterized by AFM in the high-T region [red dashed line in Fig. 2(b) corresponding to Fig. 3(b)] and FM at low T [blue dashed line in Fig. 2(b) corresponding to Fig. 3(a)].

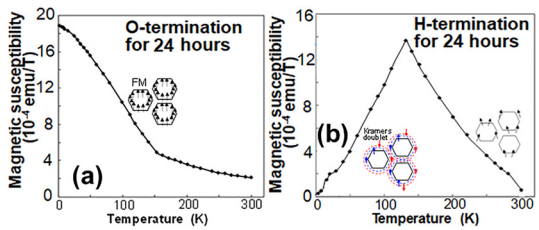

FIG. 3. Temperature dependence of magnetic susceptibilities observed at 100 Oe. (a) Completely O-terminated and (b) completely H-terminated nanomeshes. Insets: Schematic views of the possible pore-edge spin configurations.

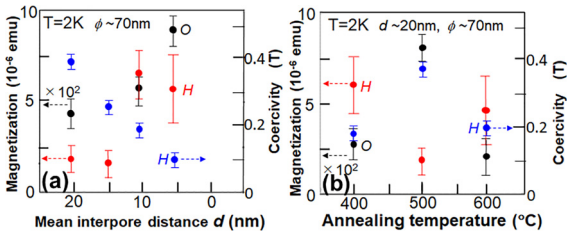

FIG. 4. Structure and annealing dependence of the magnetism of the completely H- or O-terminated nanomeshes. (a) Interpore distance (d) dependence under a constant pore diameter (ϕ) and (b) annealing temperature dependence. Red circles: magnetization values at 100 Oe in H-terminated samples (left Y-axis). Black circles: those in O-terminated samples (left Y-axis). Blue circles: coercivity in H-terminated samples (right Y-axis). The error bars correspond to the analysis of five samples with different structures and conditions.

We now discuss the causes for the observed magnetisms and the correlations with 2D TI states. The presence of 2D TI states in the present nanomeshes has not been confirmed due to the extremely small interpore space and the small pore-edge size (e.g., even for resistance and STS measurements), as mentioned above. However, the AFM was never observed in our previous non-TI nanomeshes; thus, this observation is unique to the present thin Bi_2Te_3 nanomeshes. Because the H-termination does not lead to spin splitting at the pore edges, as mentioned for our previous non-TI nanomeshes, helical edge states may remain in this case if they exist. Therefore, one possible cause of the observed AFM may be the AFM spin alignment of Kramers doublets, which may exist along the pore edges as well as along edges of the thin flakes.

In Fig. 4(a), it is found that the decrease in d leads to unstable AFM in the H-terminated nanomeshes. This is very different from the monotonic increase in FM in the O-terminated sample, which originates from the increased interaction between the two edges of an interpore region (as a nanoribbon), as mentioned below, and is consistent with our previous results, as mentioned in the introduction.[21–25] These differences support the idea that the observed AFM originates from different mechanisms and may be associated with the Kramers doublets existing at the pore edges, as mentioned above, because the decrease in d can induce interplay among the multiple Kramers doublets residing at different pore edges, which align as in a honeycomb array. The induced interplay causes AFM spin instability with a reduction in coercivity, similar to that observed in a Kagome lattice.[26,27] In Fig. 4(b), it is found that the AFM in the H-terminated samples becomes most robust after the annealing at the optimized T_a, which emphasizes that the helical edge states existing around the pore edges become most stable at the zigzag edges, consistent with Refs. 28 and 29. In previously reported 2D-TIs, AFM spin alignment was not detected due to the small volume of edges. The present 2D nanomesh structure, with its extremely large volume of pore edges (pore density $> \sim 10^{11}$ cm^{-2}), allows this observation.

In contrast, the observed FM and associated behaviors in the O-terminated nanomeshes (Fig. 4) are analogous to our previous reports on FM, which originated from the orbital coupling between the dangling-bond atoms at the zigzag pore edges and the foreign atoms terminating the edges in the nanomeshes formed on various 2D

non-TI thin layers, as mentioned in the introduction.[20–25] This origin may suggest that the cause is associated with spin splitting in the Te$3d_{5/2}$ orbital of the Te-O coupling confirmed at the pore edges [Fig. 1(f)].[32] However, the helical edge spin states of the 2D TI are topologically protected by time-reverse symmetry, as mentioned above. How the states are correlated with the termination of the edges by adatoms has not been well investigated, particularly for magnetic ordering. Only a few studies have reported that oxygen decoration of TIs modulated the Fermi levels by carrier doping and that the resistivity was reduced.[35] The present result reveals the possibility that the AFM spin alignment of the helical edge states may be suppressed by the FM spin alignment due to this edge O-termination if the observed AFM is attributed to the helical edges around the pore edges.

For the sample depicted in Fig. 3(a), oxidation was carried out for as long as 24 h. This amount of exposure is sufficient for terminating all the pore-edge dangling bonds with O atoms, resulting in the observed FM. In contrast, the oxidation time was short for the sample in Fig. 2, resulting in partial edge O-termination. Thus, the result in Fig. 2 can be interpreted as a hybridization of the phenomena presented in Figs. 3(a) and 3(b), as mentioned above.

However, it remains unclear how the AFM caused by Kramers doublets can interplay with the FM arising from spin splitting in the O-Te coupled orbitals near the partially O-terminated pore edges [Fig. 2(b)]. Two explanations for this are considered: the AFM and FM (1) separately exist in different pore edges [insets of Figs. 2(b) and 2(e)] or (2) coexist in the same pore edges. For case (1), spin localization, which originates from the strong edge O-Te coupling in the Te$3d_{5/2}$ orbitals and FM spin alignment in the orbitals, destroys the Kramers doublet at one pore edge. Even at the partially oxidized edge of one pore, this destruction occurs, causing the Kramers doublet to completely disappear. On only the pore edges without any oxidation can the Kramers doublets survive. In contrast, for case (2), the FM spin alignment of the edge O-Te coupling does not destroy the Kramers doublet. The Kramers doublets propagate along the outside of the edge O-Te coupling orbital.

The FM observed in Fig. 3(a) and the absence of AFM suggest that the former model is appropriate because the sufficient degree of O-termination realizes the formation of the edge O-Te coupling over the entire pore system of the sample. If the latter model is applicable, AFM should be observed to some extent even under such a condition. In Fig. 2(b), the oxidation time being as short as 2 h and apparently insufficient leads to the states presented in the insets of Figs. 2(b) and 2(e).

In conclusion, we have demonstrated the possibility that a large volume of Kramer doublets, which possibly exist around non-O-terminated nanopore edges of 2D Bi_2Te_3 nanomeshes, may produce AFM, but the FM spin alignment due to the O-Te coupling at the O-terminated pore edges eliminates this AFM. Interplay between the AFM and FM can appear in partially O-terminated samples. It is essential to confirm the presence of 2D TI states in the present nanomeshes. Previously, a 2D van der Waals magnet, bilayer CrI_3, enabled electric-field switching of its magnetisms due to the interlayer exchange bias.[30] Optimizing the present 2D nanomesh structures with O- or H-termination is expected to realize such control over topological magnetisms and spintronics if 2D TI states are confirmed.

We thank T. Ando, T. Yamamoto, S. Tarucha, K. Nomura, T. Enoki, J. J. Palacios, A. H. Macdonald, P. J.-Herrero, R. Wu, and P. Kim for their technical contributions, fruitful discussions, and encouragement. The work at Aoyama Gakuin University was partly supported by a grant for private universities and a Grant-in-Aid for Scientific Research (15K13277) awarded by MEXT. The work at the University of Tokyo was partly supported by Grant-in-Aid for Scientific Research (Grant No. 19H00652).

REFERENCES

[1]H. Zhang, C. X. Liu, X. L. Qu, X. Dai, Z. Fang, and S. C. Zhang, Nat. Phys. **5**, 438 (2009).
[2]Y. Xia, D. Qian, D. Hsieh, L. Wray, A. Pal, H. Lin, A. Bansil, D. Grauer, Y. S. Hor, R. J. Cava *et al.*, Nat. Phys. **5**, 398 (2009).
[3]M. Z. Hasan and C. L. Kane, Rev. Mod. Phys. **82**, 3045 (2010).
[4]M. Ye, W. Li, S. Zhu, Y. Takeda, Y. Saitoh, J. Wang, H. Pan, M. Nurmamat, K. Sumida, F. Ji *et al.*, Nat. Commun. **6**, 8913 (2015).
[5]C.-Z. Chang, J. Zhang, M. Liu, Z. Zhang, X. Feng, K. Li, L.-L. Wang, X. Chen, X. Dai, Z. Fang *et al.*, Adv. Mater. **25**, 1065 (2013).
[6]Y. Ni, Z. Zhang, I. C. Nlebedim, R. L. Hadimani, G. Tuttle, and D. C. Jiles, J. Appl. Phys. **117**, 17C748 (2015).
[7]Z. I. Wang, K. Segawa, S. Sasaki, A. A. Taskin, and Y. Ando, APL Mater. **3**, 083302 (2015).
[8]P. P. J. Haazen, J.-B. Laloë, T. J. Nummy, H. J. M. Swagten, P. Jarillo-Herrero, D. Heiman, and J. S. Moodera, Appl. Phys. Lett. **100**, 082404 (2012).
[9]J. G. Checkelsky, J. Ye, Y. Onose, Y. Iwasa, and Y. Tokura, Nat. Phys. **8**, 729–733 (2012).
[10]Y. S. Hor, P. Roushan, H. Beidenkopf, J. Seo, D. Qu, J. G. Checkelsky, L. A. Wray, D. Hsieh, Y. Xia, S.-Y. Xu *et al.*, Phys. Rev. B **81**, 195203 (2010).
[11]M. D. Watson, L. J. Collins-McIntyre, L. R. Shelford, A. I. Coldea, D. Prabhakaran, S. C. Speller, T. Mousavi, C. R. M. Grovenor, Z. Salman, S. R. Giblin *et al.*, New J. Phys. **15**, 103016 (2013).
[12]C. L. Kane and E. J. Mele, Phys. Rev. Lett. **95**, 226801 (2005).
[13]A. Roth, C. Brüne, H. Buhmann, L. W. Molenkamp, J. Maciejko, X.-L. Qi, and S.-C. Zhang, Science **325**, 294 (2009).
[14]L. J. Du, I. Knez, G. Sullivan, and R.-R. Du, Phys. Rev. Lett. **114**, 096802 (2015).
[15]S. Tan, C. Zhang, D. Wong, Z. Pedramrazi, H.-Z. Tsai, C. Jia, B. Moritz, M. Claassen, H. Ryu, S. Kahn *et al.*, Nat. Phys. **13**, 683 (2017).
[16]S. Wu, V. Fatemi, Q. D. Gibson, K. Watanabe, T. Taniguchi, R. J. Cava, and P. J. Herrero, Science **359**, 76 (2018).
[17]H. Mine, A. Kobayashi, T. Nakamura, T. Inoue, S. Pakdel, E. Z. Marin, D. Marian, S. Maruyama, S. Katsumoto, J. Haruyama *et al.*, "Laser-beam patterned topological insulating states on thin semiconducting MoS2," Phys. Rev. Lett. (to be published).
[18]J. Hu, J. Alicea, R. Wu, and M. Franz, Phys. Rev. Lett. **109**, 266801 (2012).
[19]T. Nanba, K. Tamura, K. Hatsuda, T. Nakamura, C. Ohata, S. Katsumoto, and J. Haruyama, Appl. Phys. Lett. **113**, 053106 (2018).
[20]K. Hatsuda, H. Mine, T. Nakamura, J. Li, R. Wu, S. Katsumoto, and J. Haruyama, Sci. Adv. **4**, eaau6915 (2018).
[21]J. Haruyama, Electronics **2**, 368 (2013).
[22]T. Hashimoto, J. Haruyama, D. Soriano, and S. Roche, Appl. Phys. Lett. **105**, 183111 (2014).
[23]Y. Nakanishi1, A. Ishi, C. Ohata, D. Soriano, R. Iwaki, K. Nomura, M. Hasegawa, T. Nakamura, S. Katsumoto, and S. Roche, Nano Res. **10**, 718 (2017).
[24]C. Ohata, R. Tagami, Y. Nakanishi, R. Iwaki, K. Nomura, and J. Haruyama, Appl. Phys. Lett. **109**, 133110 (2016).
[25]G. Kondo, N. Yokoyama, S. Yamada, Y. Hashimoto, C. Ohata, S. Katsumoto, and J. Haruyama, AIP Adv. **7**, 125019 (2017).
[26]J.-X. Yin, S. S. Zhang, H. Li, K. Jiang, G. Chang, B. Zhang, B. Lian, C. Xiang, I. Belopolski, H. Zheng *et al.*, Nature **562**, 91 (2018).
[27]A. Vasiliev, O. Volkova, E. Zvereva, and M. Markina, NPJ Quantum Mater. **3**, 18 (2018).
[28]K. Imamura, A. Yamakage, S. Mao, A. Hotta, and Y. Kuramoto, Phys. Rev. B **82**, 085118 (2010).
[29]K. Imamura, S. Mao, A. Yamakage, and Y. Kuramoto, Nanoscale Res. Lett. **6**, 358 (2011).
[30]S. Jiang, J. Shan, and K. F. Mark, Nat. Mater. **17**, 406 (2018).

[31]NPATs are synthesized according to our previous method of anodic oxidation of a pure aluminium substrate, with optimized conditions. The NPAT is closely attached to the abovementioned thin Bi_2Te_3 flakes on a SiO_2/Si substrate, and the flakes are carefully etched by Ar gas under low power to avoid damaging the pore edges. Then, the NPAT is mechanically detached.
[32]In particular, few-layer MoS_2 nanomesh with zigzag-pore-edge dangling bonds terminated by O atoms demonstrated FM depending on the structure and annealing temperature used.25 The Mo dangling bonds at the pore edges had unsaturated bonds in the core $3d_{3/2}$ and $3d_{5/2}$ orbitals. The O-termination of these unsaturated bonds led to significant spin splitting and the observed FM. The FM observed here should be qualitatively analogous to this mechanism because the Te$3d_{5/2}$ orbital in the Te-O coupling has been confirmed.
[33]C.-X. Liu, H. Zhang, B. Yan, X.-L. Qi, T. Frauenheim, X. Dai, Z. Fang, and S.-C. Zhang, Phys. Rev. B **81**, 041307R (2010).
[34]Y. Y. Li, G. Wang, X. G. Zhu, M. H. Liu, C. Ye, X. Chen, Y. Y. Wang, K. He, L. L. Wang, X. C. Ma *et al.*, Adv. Mater. **22**, 4002 (2010).
[35]K. Hoefera, C. Beckera, D. Rataa, J. Swansona, P. Thalmeiera, and L. H. Tjenga, Proc. Natl. Acad. Sci. **111**, 14979 (2014).